Nonlinear dynamics of nonadiabatic chirping-frequency Alfvén modes in tokamak plasmas

OPEN ACCESS
IOP Publishing
Plasma Physics and Controlled Fusion
Plasma Phys. Control. Fusion **65** (2023) 074001 (15pp)
https://doi.org/10.1088/1361-6587/acd71f

Nonlinear dynamics of nonadiabatic chirping-frequency Alfvén modes in tokamak plasmas

X Wang[1,*], S Briguglio[2], A Bottino[1], M Falessi[2], T Hayward-Schneider[1], Ph Lauber[1], A Mishchenko[3], L Villard[4] and F Zonca[2,5]

[1] Max Planck Institute for Plasma Physics, Garching D-85748, Germany
[2] ENEA, Fusion and Nuclear Safety Department, C. R., Frascati, Via Enrico Fermi 45 C. P. 65 - I-00044 - Frascati, Italy
[3] Max Planck Institute for Plasma Physics, Greifswald D-17491, Germany
[4] Ecole Polytechnique Fédérale de Lausanne (EPFL), Swiss Plasma Center (SPC) CH-1015 Lausanne, Switzerland
[5] Institute for Fusion Theory and Simulation, School of Physics, Zhejiang University, Hangzhou, People's Republic of China

E-mail: xin.wang@ipp.mpg.de

Received 27 February 2023, revised 16 May 2023
Accepted for publication 19 May 2023
Published 30 May 2023

Abstract

Frequency chirping of Alfvén modes, a phenomenon observed in tokamak fusion plasmas driven by energetic particles (EPs), can result in significant losses of EPs. In this study, we use the global gyrokinetic code ORB5 (Lanti *et al* 2020 *Comput. Phys. Commun.* **251** 107072) to investigate the nonlinear dynamics of non-adiabatic frequency chirping EP modes (EPMs). Our results illuminate non-perturbative features of EPMs caused by the presence of EPs. Additionally, we find that, with a fixed safety factor profile and a single toroidal mode number, the frequency chirping rate is linearly proportional to the mode saturation amplitude, as predicted by the theory (Chen and Zonca 2016 *Rev. Mod. Phys.* **88** 015008).

Keywords: energetic particles, gyrokinetic, Alfvén mode

(Some figures may appear in colour only in the online journal)

1. Introduction

Frequency chirping refers to the phenomenon where the frequency of a wave changes over time. It is observed in both space plasmas and laboratory plasmas. In space plasmas, for example, frequency chirping is commonly observed in the form of chorus waves, which are electromagnetic waves that occur in Earth's radiation belts and in the magnetosphere of other planets. These waves are characterized by a frequency that increases over time due to nonlinear wave-particle interaction, which is an important mechanism in the generation of chorus waves (cf e.g. [1, 2]). Understanding the properties and behavior of these waves is crucial for improving our understanding of the magnetosphere and radiation environment around Earth and other planets.

In tokamak plasmas, Alfvén eigenmodes (AEs) are electromagnetic oscillations existing within the frequency gaps of the shear Alfvén continuous spectrum. These modes can be excited by the presence of high-energy particles known as energetic particles (EPs). EPs can be created in tokamak plasmas through various mechanisms, such as fusion reactions or neutral beam injection. They can interact with the Alfvén modes and cause the frequency of the oscillation to change.

* Author to whom any correspondence should be addressed.

This can affect the transport of the particles and influence the distribution of energy and particles within the plasma (cf e.g. [3] for a recent review). The study of frequency chirping of Alfvén modes driven by EPs is a crucial area of research in Fusion plasmas and is of particular interest in our work. Understanding this phenomenon is important for improving our understanding of the behavior of plasmas in fusion devices and for developing strategies to control these modes. Note that in tokamak fusion plasmas, the term 'frequency chirping' refers to a change in frequency on a timescale that is typically shorter than the evolution of background plasma parameters. It's important to note that the latter, which is sometimes referred to as 'sweeping', which is not addressed in this paper.

There are currently two paradigms for discussing nonlinear interactions of Alfvénic fluctuations with EPs in fusion plasmas [4, 5], namely the bump-on-tail and the fishbone paradigms. The bump-on-tail paradigm can be adopted when the system is sufficiently close to marginal stability and the nonlinear changes of resonant EP orbits are small compared to the characteristic fluctuation wavelength [6, 7]. This model can only account for local EP transport in the presence of an isolated resonance, unless the threshold is exceeded for the onset of stochasticity in the particle phase space due to overlapping resonances. The essential physics of the bump-on-tail paradigm are the same as those first introduced to analyze the temporal evolution of a small cold electron beam interacting with a plasma in a 1D system [8, 9]. The dynamics of the nonlinear beam-plasma system with sources and collisions [6, 7, 10] include steady-state and bursting behaviors [11–13], the formation of hole and clump pairs in the resonant particle phase space [13–15], and the existence of subcritical states [15]. Applications of the 1D bump-on-tail paradigm to AEs are used to explain the experimental observations such as frequency splitting of AE spectral lines [16], and adiabatic frequency chirping of the modes [17–19], where the rate of frequency change is much slower than the wave-particle trapping frequency $|\dot{\omega}| \ll \omega_B^2$. Numerical simulations of the bump-on-tail system have demonstrated that structures can be formed and propagate in the phase space as BGK modes [20], characterized as long-range frequency sweeping events with corresponding convective (bucket) particle transport [21–24]. Such structures also exist away from marginal stability [25], where, however, the plasma non-uniformity effect becomes increasingly more important and non-perturbative EP dynamics eventually requires a paradigm shift toward the so-called fishbone paradigm [5, 26].

The fishbone paradigm is a way of understanding the non-adiabatic chirping of AEs in tokamak plasmas. Unlike the bump-on-tail paradigm, it does not require the adiabatic assumption to be valid. The theory of non-adiabatic chirping is very well established and addresses self-consistently nonlinear fluctuation dynamics and EP transport, treated on the same footing taking into account toroidal geometry and plasma nonuniformity. Furthermore, it recovers the bump-on tail paradigm near marginal stability and, thus, provides a unified theoretical framework for investigating both adiabatic and non-adiabatic frequency chirping events as well as perturbative and non-perturbative EP responses to nonlinear dynamic evolution of the fluctuation spectrum [3, 5]. In reference [5], as an application of this unified theoretical framework, the nonlinear theory of frequency chirping EP modes (EPMs) is developed and the corresponding EP transport due to EPMs is investigated [26]. The comprehensive review paper [3] further develops the nonlinear theory of fishbones, building on earlier work [27]. The fishbone paradigm is particularly useful to explore the connection with the bump-on-tail paradigm, since it reduces the self-consistent wave-particle interaction to a time-dependent non-uniform system with one degree of freedom, which is described by means of a Dyson-like equation. Removing the non-uniformity sets an upper bound on the strength of the mode drive and allows recovering the standard bump-on-tail system in the perturbative limit [5, 26].

The objective of this study is to gain an understanding of the fundamental characteristics of non-adiabatic frequency chirping modes and provide numerical evidence of the underlying physics, comparing simulation results with the existing unified theoretical framework. To achieve this, we will review the theoretical explanations for both adiabatic and non-adiabatic frequency chirping in section 2. We will use recent phase space analysis from numerical simulations as evidence and present the theoretical predictions for frequency chirping rates. In section 3, we will illuminate the frequency chirping of non-perturbative EPMs using first-principle gyrokinetic simulations from the ORB5 code [28]. By focusing on a single mode and varying different parameters, we will demonstrate the relationship between the frequency chirping rate and the mode saturation amplitude. Note that, our current simulations use an analytical equilibrium, which is easier to manipulate by adding more physics and serves as a numerical experiment rather than an attempt to explain any specific experimental results. Such numerical settings can easily be used as a benchmark case for any code. Finally, in section 4, we will summarize the key findings and conclusions from this study.

2. Adiabatic chirping vs. nonadiabatic chirping

2.1. Theoretical explanation

Alfvén fluctuations in burning plasmas are characterized by low amplitudes, $|\delta \mathbf{B}_\perp|/B_0 \lesssim 5 \times 10^4$, and predominantly perpendicular variation with respect to the equilibrium magnetic field [29]. Resonant particles are expected to play a crucial role in transport processes [30–34] more so than non-resonant particles. Therefore, phase space structures that are obtained by averaging out dependencies on two periodic angle-like coordinates (θ, ζ) in two-dimensional (2D) magnetized plasma equilibria are of particular interest in studying transport processes. These structures are commonly referred to as phase space zonal structures (PSZS) [3, 5, 35, 36]. The dynamics of these structures are affected by the relative ordering of two time scales: the wave-particle trapping time, τ_B, and the characteristic time of nonlinear evolution of PSZS, τ_{NL}. When $\tau_B \ll \tau_{\mathrm{NL}}$, there is an adiabatic (action) invariant, phase space density is preserved inside the structure separatrix, and

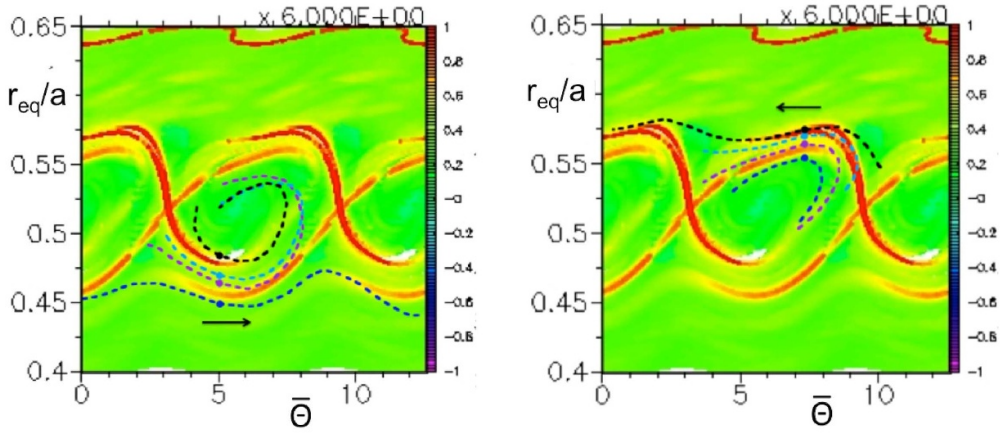

Figure 1. The x coordinate $\bar{\Theta}$ refers to the wave-particle phase, and the y coordinate r_{eq}/a refers to the normalized minor radius at the equatorial plane. Lagrangian Coherent Structures are displayed in red, while selected particle trajectories are illustrated using dashed lines (refer to figures 23 and 24 in [50]. The trajectories of initially trapped particles, such as the the purple trajectory in the left panel illustrate the process of trapping and detrapping. Reproduced from [Physics of Plasmas 29, 032 512 (2022), https://aip.scitation.org/doi/10.1063/5.0080785], with the permission of AIP Publishing. Reproduced from [50]. CC BY 4.0.

phase space holes and clumps [20, 37–41] form and propagate in the phase space. This nonlinear evolution is referred to as adiabatic and particle transport can be secular and extend over a long range [21–23] in the sense of bucket transport [42]. On the other hand, when $\tau_B \sim \tau_{\rm NL}$, no adiabatic invariant exists in the phase space, resonant particle motion can be secular and the dynamics is referred to as nonadiabtic. Similar to the adiabatic regime, a phase space region where particles remain trapped is still possible in the nonadiabatic sweeping case, but generally particles get synchronized and de-synchronized (or, loosely speaking, trapped and detrapped) with the phase space structure. Existence of these particles is of crucial importance and fundamental nature [43], and, as a results, it has a big impact on the self-consistent nonlinear evolution [1–3, 5, 44]. Thus, different nonlinear behaviours and EP transport are expected depending the relative ordering of τ_B and $\tau_{\rm NL}$.

2.2. Numerical demonstration of trapping and detrapping process

In [45–48], the authors utilize a Lagrangian methodology to delineate transport barriers within the system, employing the Lagrangian Coherent Structures technique [46, 47]. It can be demonstrated that these structures can be described by peaked profiles of the Finite Time Lyapunov Exponent fields [47]. These (hyperbolic) Lagrangian Coherent Structures act as transport barriers for the tracers, classifying them into two distinct categories of evolution, namely trapped and untrapped particles by a wave. The Hamiltonian mapping technique has been widely developed to understand the nonlinear dynamics of frequency chirping Alfvén modes driven by energetic particles [49]. This technique divides the phase space into slices that are orthogonal to the invariant coordinates, preventing particle flux between slices and allowing for separate investigations of each slice. In a recent study [50], theses techniques are combined to examine the detailed dynamics of particle dynamics in the phase space. In figure 1 (also seen in figures 23 and 24 of [50]), we show various particle trajectories, illustrating that channels are present between the attractive and repulsive lines. These channels enable the inflow of particles from the lower edge and outflow of particles from the upper edge of the coherent structure, as exemplified by the purple trajectory in figure 1. These findings can be easily explained by the identified trapping and detrapping process. Additionally, it should be noted that this trapping and detrapping process accompanying chirping fluctuations has recently been observed in hybrid simulations [1] of 'chorus emission' in the Earth's magnetosphere, suggesting the universal nature of the underlying nonlinear dynamics [2, 3].

2.3. Frequency chirping rate

In the adiabatic limit, the bump-on-tail paradigm (also known as 'BB' model) yields a quantitative prediction of the chirping rate if the value of γ_L and γ_d are known [14, 15], where γ_d represents damping and γ_L represents the kinetic drive by EPs. With some approximations, their integral relation between $\delta\omega$ and ω_b reduces to the analytical form

$$\delta\omega^{BB} = \omega_b^{BB}\left(\frac{2\gamma_d}{3}t\right)^{1/2} \approx 0.44\times\gamma_L(\gamma_d t)^{1/2}. \qquad (1)$$

However, as the demonstrated by the generalized fishbone like dispersion relation (GFLDR) [3], the EP contribution is non-perturbative and can significantly affect the mode structure and nonlinear frequency chirping, breaking the assumptions used in the one-dimensional bump-on-tail problem.

As the strength of the EP source increases, non-perturbative EP effects become more visible on both AEs and EPMs in magnetized plasmas [51–54]. EPMs, in particular, are excited at the resonant EP characteristic frequency [55] and are localized near the maximum of the resonant EP drive [51, 56]. This allows for maximum power exchange between the waves and EPs by preserving the resonance condition throughout

the nonlinear evolution, a process known as 'phase locking'. Recent studies have shown these effects in experimental measurements of the toroidal Alfvén eigenmode (TAE) mode structures in DIII-D, in comparison with numerical simulation results [57]. Additionally, 'phase locking' is intrinsically connected with non-adiabatic frequency chirping of EPMs, as the frequency adapts to the local resonance condition, following [3, 5]

$$\dot{\omega} \simeq \delta\dot{\mathbf{X}}_{\perp} \cdot \nabla\omega_{\rm res} \ , \tag{2}$$

where $\delta\dot{\mathbf{X}}_{\perp}$ is the fluctuation induced EP velocity and $\omega_{\rm res}$ is the space-dependent resonance frequency. Frequency chirping described by equation (2) is an expression of the intrinsic nature of nonlinear EPM dynamics, known as the 'intrinsic autoresonance'. This is different from the typical concept of 'autoresonance,' where the drive frequency is controlled externally, as stated in [58, 59]. The term 'phase locking' is commonly used to describe the instantaneous matching of the nonlinear oscillator frequency with that of the external drive in the case of 'autoresonant' nonlinear evolution of phase space holes/clumps, as mentioned in [58, 59]. In addition, 'phase locking' has also been used to describe the slow (adiabatic) evolution of phase space holes/clumps that move to a lower energy state and compensate for energy dissipation due to background damping, as stated in [60]. This confirms the analogy of theories on adiabatic frequency sweeping of holes/clumps, as stated in [12–15, 60, 61], with the concept of 'autoresonance' [58, 59]. In both cases, the shortest nonlinear time scale is determined by wave-particle trapping and the conservation of the corresponding phase space invariant on the longer time scale. However, equation (2) highlights the distinct nature of 'phase locking' when there is a sufficiently strong instability drive and non-perturbative EP response. In this case, in fact, $\delta\dot{\mathbf{X}}_{\perp}$ is self-consistently set by the fluctuation induced EP velocity, consistent with the non-perturbative nature of the EP response; while in the adiabatic case $\dot{\omega}$ and, thus, $\delta\dot{\mathbf{X}}_{\perp}$ is controlled externally (or by a slower perturbative process) [3, 5]. In this scenario, the wave-particle phase evolves slowly on the shortest nonlinear time scale and wave-particle trapping is suppressed [3, 5, 26, 49, 62, 63]. In the latter, we conduct simulations using ORB5 code [28] to investigate the evidence and demonstrate the relationship between the chirping rate and the amplitude, as indicated in equation (2).

3. Simulation results

3.1. Nonlinear initial value gyrokinetic code ORB5

Numerical simulations are performed using ORB5 [28], a global, electromagnetic, particle-in-cell (PIC), gyrokinetic code that incorporates collisions and sources. These simulations are used to validate the theoretical predictions discussed in section 2. ORB5 is the ideal numerical tool for investigating dynamics driven by EPs, as it maintains a kinetic description of all species and effectively describes wave-particle interactions. ORB5 [28, 64, 65] implements the most comprehensive physical model available. It employs the Monte Carlo Lagrangian PIC method for evolving the distribution function, which is sampled using markers, and the fields (electrostatic and electromagnetic potentials) are solved on a grid using finite element representation.

The ORB5 code solves the gyrokinetic Vlasov equation, which is coupled with the relevant gyrokinetic field equations, including a polarization equation (Poisson) and, in the electromagnetic model, a parallel Ampére's law [28]. The gyrokinetic Vlasov equation for particle species s, in the absence of collisions and sources, describes the distribution function of the particles and reads:

$$\frac{{\rm d}f_s}{{\rm d}t} = 0 \ , \tag{3}$$

${\rm d}/{\rm d}t$ is the convective derivative. The full derivation of the GK model of ORB5 can be found in [66]. The distribution function is then decomposed into an analytically known background f_0, solution of the unperturbed Vlasov equation, and a perturbed distribution functions δf . The Vlasov equation becomes now an evolution equation for δf

$$\frac{{\rm d}\delta f_s}{{\rm d}t} = -\frac{{\rm d}f_{0s}}{{\rm d}t} \ , \tag{4}$$

where f_{0s} is typically written as a function of the kinetic energy, the adiabatic invariant per unit mass μ and the gyrocenter position R.

The nonlinear global electromagnetic gyrokinetic Lagrangian model of the code, as outlined in [66], is extensively discussed in [28, 65, 67]. However, for the purpose of this work, we have only provided a brief overview of the key components and focus on the details most relevant simulation results.

3.2. Equilibrium and other simulation parameters

3.2.1. Equilibrium. We examine a tokamak geometry with an aspect ratio of $A = 10$ and concentric circular cross-sections. The safety factor is defined as $q(\rho) = 1.4 + 0.1\rho - 0.25\rho^2 + 0.2\rho^3 + 1.9\rho^4$, where ρ is the radius of the circular flux surface. An ad-hoc tokamak equilibrium is employed, defined by the relations $\mathbf{B} = \nabla\psi \times \nabla\varphi + I\nabla\varphi$, where $I = B_0R_0$, $\psi(\rho) = \int_0^{\rho} B_0\rho' d\rho'/q(\rho')$, and φ is the toroidal angle. The magnetic field on the axis is $B_0 = 3.0$T, and the major radius is $R_0 = 10.0$m. The temperature profile for the bulk plasmas is assumed to have the following forms:

$$T_{0(i,e)}(s)/T_{0(i,e)}(s=0.5) = \exp\left[\frac{\kappa_T\Delta_T}{2.0}\log\left(\frac{\cosh\left(\frac{s-0.9}{\Delta_T}\right)}{\cosh\left(\frac{s-0.1}{\Delta_T}\right)}\right)\right]. \tag{5}$$

Here, $s = \sqrt{\psi/\psi_a}$, where ψ is the poloidal magnetic flux and ψ_a is the poloidal magnetic flux at the plasma edge. For the bulk ion density profile, it is assumed to be uniform for all simulations. Once the EP population is loaded into the simulation code, ORB5 chooses to satisfy quasineutrality for the

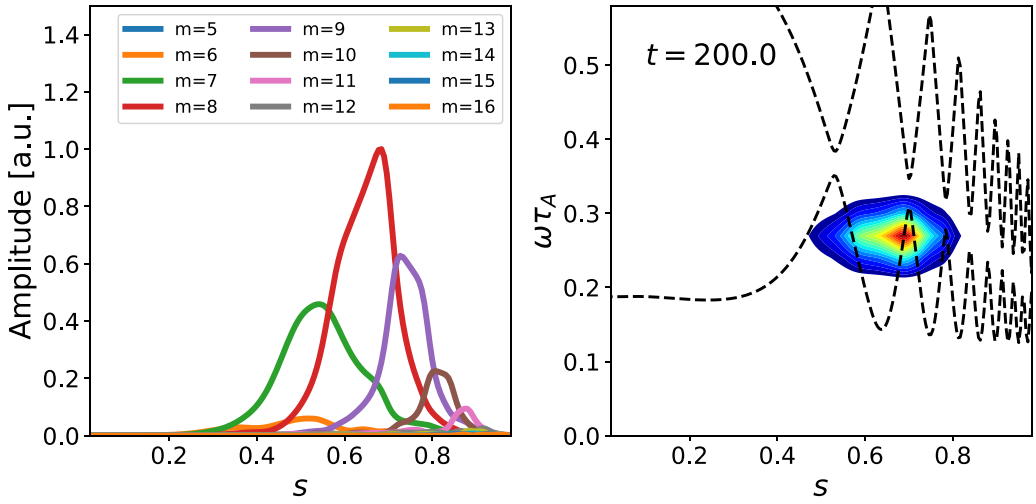

Figure 2. The mode features during the linear stage at $t = 200\tau_A$. Left: radial structure of the poloidal harmonics of the mode. Rigth: spectrum of the scalar potentail in space (s, ω). The black dashed lines are the shear Alfvén continua, which are calculated in the ideal MHD limit [70] using the slow sound approximation [71] with an effective kinetic pressure [72] to properly account for the geodesic compressibility.

considered simulations. This means that the code automatically calculates the electron density profile, in order to achieve $n_e = n_i + n_{EP}$ at any radial position. For the bulk plasma temperature profile, $s_0 = 0.5$ is fixed, but different values of κ_T are considered in different simulations. The ion and electron temperatures are taken to be equal everywhere: $T_e = T_i$. For EPs, the density profile have the following form:

$$n_{0h}(s)/n_{0h}(s_0) = \exp\left[-\kappa_n \Delta_n \tanh\left(\frac{s - s_0}{\Delta_n}\right)\right], \qquad (6)$$

where $s_0 = 0.62$, $\kappa_n = 3.333$ and $\Delta_n = 0.1$ are used to produce a density gradient drive. The machine size is determined by $L_x = 2r_a/\rho_s = 350$ with r_a the minor radius and ρ_s the characteristic sound Larmour radius, the ion-to-electron mass ratio is $m_i/m_e = 200$. The parameter $\beta_e = 2\mu_0 n_e T_{0e}(s = 0.5)/B_0^2 = 0.0043$ is fixed.

3.2.2. EP initial distribution function. The distribution function of the EP population is an analytical slowing-down distribution function with pitch-angle dependence [68]. The distribution function is a function of energy and parallel velocity, both normalized with respect to the sound speed $v_s = \sqrt{T_e/m_i}$, where T_e is the electron temperature and m_i the ion mass:

$$f(v, \xi, \psi) = \hat{n}(\psi) \frac{2\sqrt{2/\pi}}{\sigma_\xi \left[\mathrm{erf}\left(\frac{\xi_0+1}{\sqrt{2}\sigma_\xi}\right) + \mathrm{erf}\left(\frac{\xi_0-1}{\sqrt{2}\sigma_\xi}\right)\right]} \times \exp\left(-\frac{(\xi - \xi_0)^2}{2\sigma_\xi^2}\right) \frac{3\Theta(v_\alpha - v)}{4\pi(v_c^3(\psi) + v^3)} \times \ln\left(1 + \frac{v_\alpha^3}{v_c(\psi)^3}\right). \qquad (7)$$

The analytical distribution function was obtained by multiplying a slowing-down distribution in energy, characterized by the absolute value of velocity $v = \sqrt{2\mathcal{E}}$, and a Gaussian distribution in $\xi = v_\parallel/|v|$ (where ξ can range from -1 to 1) centered at ξ_0 and characterized by a width σ_ξ. The Heaviside function $\Theta(v_\alpha - v)$ is defined as 1 for values of $v < v_\alpha$ and 0 elsewhere, where v_α is the injection velocity and $v_c(\psi)$ is the critical velocity [69], calculated from $T_e(\psi)$. The parameter $\hat{n}(\psi)$ is the local value of the normalized density. Note that, the derivatives used in the delta-f method for evolving the Vlasov equation, $\mathrm{d}f/\mathrm{d}\mathcal{E}, \mathrm{d}f/\mathrm{d}\psi, \mathrm{d}f/\mathrm{d}v_\parallel$ are calculated numerically using forward derivatives, holding the other two variables constant. In the special case of the derivative with respect to energy, we fix $\mathrm{d}f/\mathrm{d}\mathcal{E} = 0$ if $f(\mathcal{E}, v_\parallel, \psi) = 0$ or $f(\mathcal{E} + \delta\mathcal{E}, v_\parallel, \psi) = 0$. In all simulations, the EP injection energy $E_h/T_e = 84.14$, $\xi_0 = 1.0$ and $\sigma_\xi = 0.05$ are fixed. This implies that the EPs in our simulations are deeply co-passing particles, and the injection energy does not depend on the radial position. Moreover, the critical velocity is determined by the bulk plasma parameter.

3.2.3. Normalization. Time scales are normalized to the ion cyclotron frequency, $\omega_{ci} = q_i B_0/m_i c$. When measuring frequencies of Alfvénic modes simulated with ORB5, we shall convert these frequencies to units of the Alfvén frequency, $\omega_A = v_A(0)/R_0$ and the time to units of the Alfvén time, $\tau_A = \omega_A^{-1}$.

3.3. The reference case

In this section, a base case is presented and later on, comparisons are made by varying different parameters. In this base case, a single mode with toroidal mode number $n = 5$ and an on-axis density ratio of $n_{EP}/n_i = 0.008$ is shown. In figure 2, the linear radial mode structure and linear mode frequency are displayed. On the left, the radial mode structure plots indicate that the mode is dominated by the poloidal mode $m = 8$, with $m = 7$ and $m = 9$ being subdominant. On the right, it is shown that the mode's linear frequency is located on the shear Alfvén

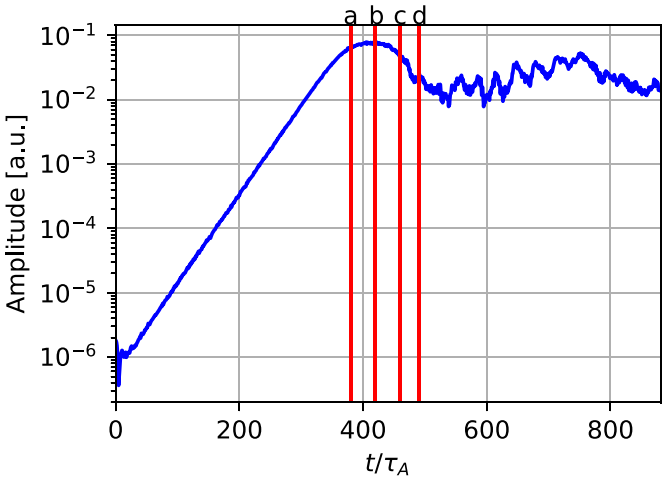

Figure 3. Time evolution of the mode amplitude at the peak. The red vertical lines indicate different times, which are a: $t = 380.0\tau_A$, b: $t = 420.0\tau_A$, c: $t = 460.0\tau_A$ and d: $t = 490.0\tau_A$, respectively.

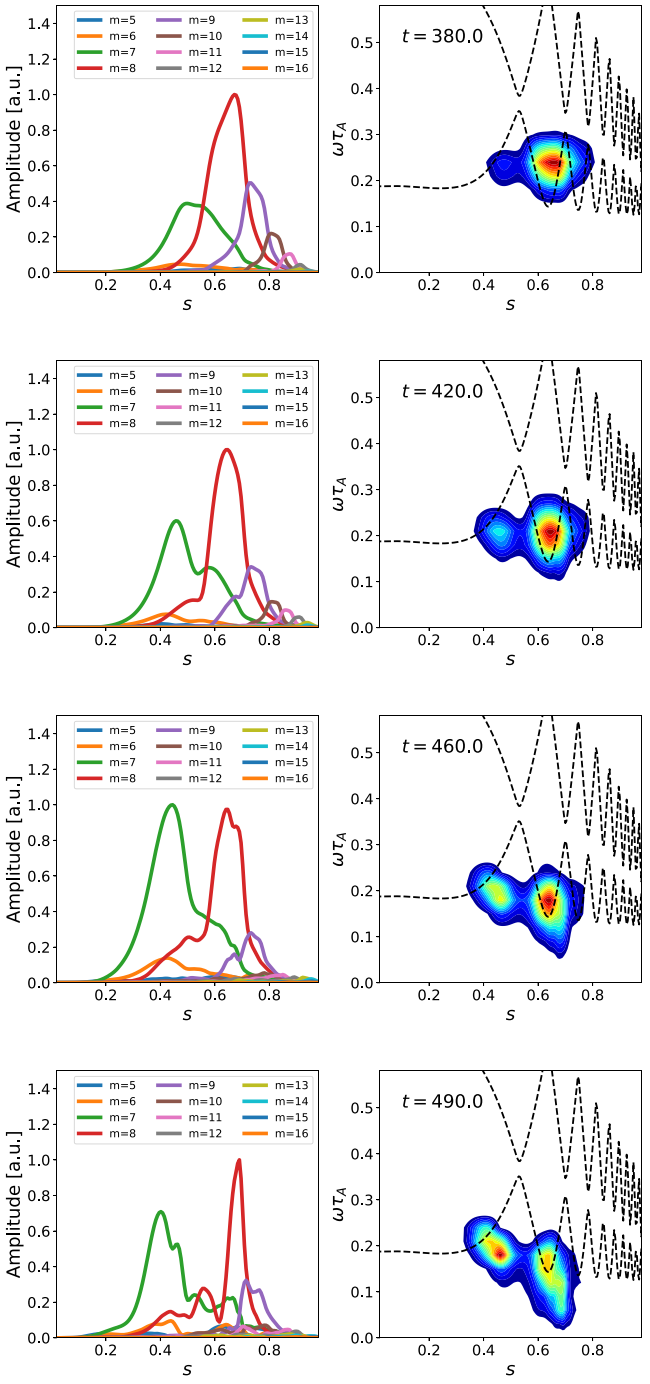

Figure 4. Four snapshots of the mode evolution at nonlinear stage. On the left, the radial mode structures are shown. Three poloidal harmonics are dominant, which are green for $m = 7$, red for $m = 8$ and purple for $m = 9$. On the right, the frequency sprectra are shown.

continuum and is close to the lower TAE accumulation point, which is recognized as an EPM. The mode's amplitude evolution is shown in figure 3, where the amplitude reaches saturation and then damps to a lower amplitude. Four snapshots of the radial mode structures and frequencies at different times (as indicated by the red vertical lines in figure 3) are shown in figure 4.

In figure 4, snapshots are shown starting from the time when the mode reaches saturation until the time when the amplitude is strongly reduced. The frequency of the mode moves downward closely following the shear Alfvén continuum. As the frequency chirps, the mode amplitude is strongly modified and self-consistently adjusted, displaying the characteristic non-adiabatic feature. The downward chirping frequency is dominated by the $m = 8$ poloidal harmonic. The $m = 7$ poloidal harmonic moves further inward radially and tends to follow its continuum. When the frequency chirps to the lower gap, the $m = 7$ harmonic decouples from the dominant $m = 8$ harmonic.

More details are shown in figure 5. The left plot shows the peak amplitude time evolution of the three most dominant poloidal harmonics. The $m = 8$ harmonic is always the most dominant one. In the linear phase, the $m = 9$ harmonic has a larger amplitude than the $m = 7$ one. In the nonlinear phase, the $m = 9$ harmonic reaches its maximum first, while the amplitude of the $m = 7$ harmonic is continuously enhanced after the $m = 8$ harmonic reaches its maximum. Meanwhile, on the right plot, it is shown that both $m = 7$ and $m = 8$ harmonic peaks drift clearly towards inner radial positions during the chirping phase, indicating that the self-consistent modification of the radial mode structure is essential for the dynamics of the mode frequency chirping, consistent with the picture of EP avalanches induced by EPMs [3, 5].

In figure 6, the frequency time evolution is displayed. The frequency spectrum is calculated by using the moving window fast Fourier transform (FFT) for all poloidal harmonics. The contour plot is produced by integrating the multi-dimensional FFT spectrum along both poloidal harmonics and radial positions. The frequency spectrum shows a clear linear dependence on time. The slope of the black dashed line is used to calculate the frequency chirping rate.

In figure 7, the normalized EP density profile at $t = 600.0$ is plotted and compared with the initial density profile. Despite no strong redistribution being observed, there is still a finite

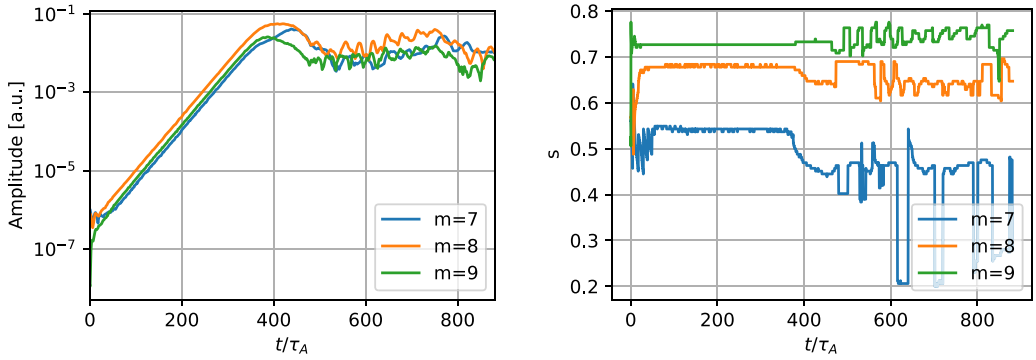

Figure 5. On the left, the time evolution of the scalar potential for the most dominant poloidal harmonics at the peak of their radial fluctuation structure are shown. On the right, the time evolution of the peak locations for each poloidal harmonic are shown.

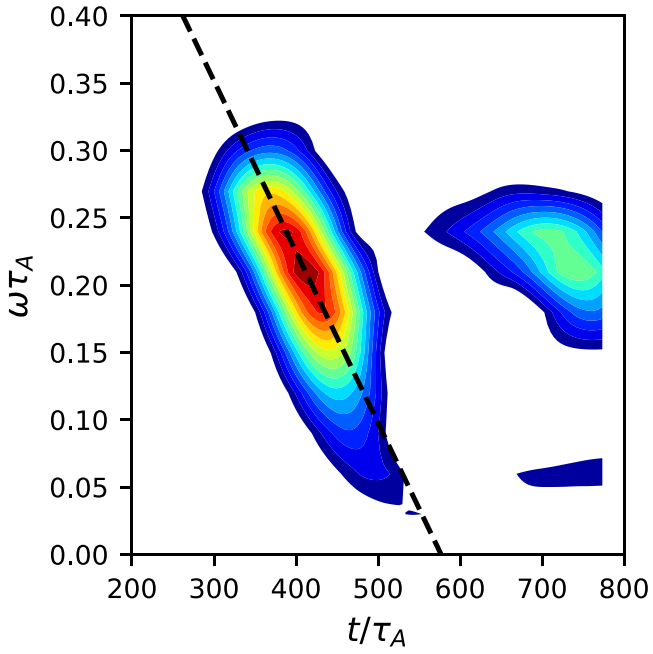

Figure 6. The frequency spectrum vs. time is shown. The linear function of the dashed line is calculated by the peak of the frequency spectrum. The slope of the dashed line indicates the frequency chirping rate.

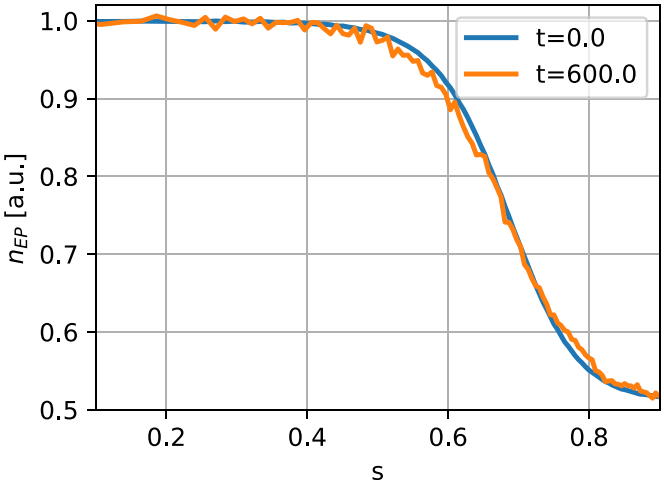

Figure 7. Normalized EP density profile at the initial time and at $t = 600\tau_A$.

modification around the mode location. The small redistribution of the total density profile is commonly observed in single-n simulations (e.g. as shown in [49]). To obtain a clearer vision of the nonlinear distortion of the density profile, it is necessary to cut the phase space into slices [49].

3.4. Drift kinetic vs. gyrokinetic

In this section, we compare the effects of using a drift-kinetic model for both thermal ions and EPs by ignoring the finite Larmor radius effect in ORB5 [73]. This approach is made possible by the flexible model implemented in ORB5 [28], which allows for numerical simulations to be carried out using the drift-kinetic limit. As previously established in literature [3], we found that the growth rates and saturation levels are modified when using the drift-kinetic model, but the mode structure and linear frequency remain unchanged, consistent with previous observations in [74]. Additionally, we observed that the frequency chirping behavior is also modified accordingly. In figure 8, we show that when comparing to the reference case where both thermal ions and EPs are treated using the gyrokinetic model, the growth-rate increases when ignoring the Larmor radius effect for EPs only, but decreases when ignoring the Larmor radius effect for thermal ions only. The saturation level, which refers to the first peak of the amplitude, is higher for larger growth rates. The frequency chirping behaviors for each case are qualitatively in agreement. As shown in figure 9, the chirping rates increase as the saturation amplitude becomes larger.

3.5. EP density scan

In this section, the results of varying the EP density while keeping the bulk plasma temperature gradient fixed at $\kappa_T = 0.5$ are presented. Increasing the EP density modifies the intensity of the EP drive while keeping the EP resonances and characteristic frequencies unchanged. In figure 10(a), the real frequencies are shown. The linear mode frequency is the same for different EP densities. In figure 10(b), the growth rates

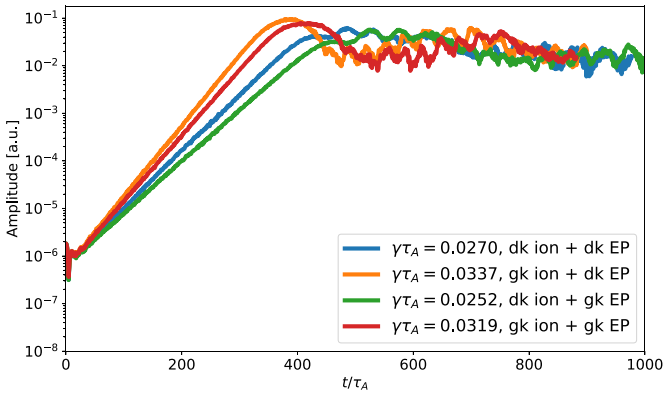

Figure 8. Mode amplitude evolution for different treatments of EP and thermal ions.

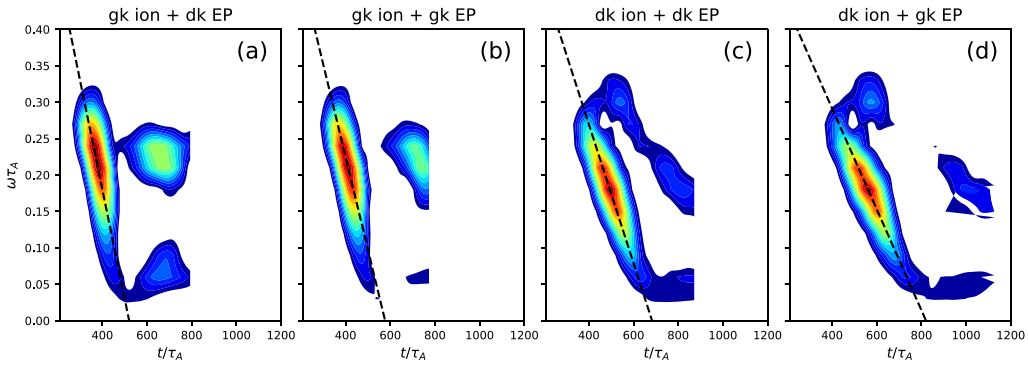

Figure 9. Mode frequency spectrum vs. time for different treatments of EP and thermal ions.

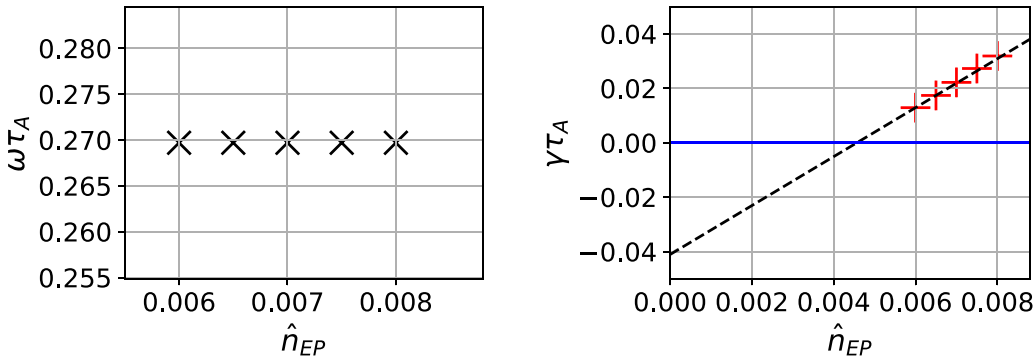

Figure 10. On the left, the linear mode frequencies are shown for EP density scan. On the right, the corresponding growth rates are shown.

are shown for scanning the EP density. The growth rates are proportional to the EP density, therefore, the damping rate and threshold density can be estimated from the dashed black line in figure 10(b). In this particular case, the damping rate $\gamma_d\tau_A = 0.0046$ and the threshold EP density is $n_{EP} \simeq 0.041$. The mode is radially located at $0.4 \leqslant s \leqslant 0.85$, with a dominant $m = 8$, and subdominant $m = 7$ and 9 poloidal Fourier components for the electrostatic field ϕ, and located in the frequency spectrum with a frequency close to the lower accumulation point of a TAE gap on the shear Alfvén continuous spectrum.

In figure 11, the time evolution of the mode amplitudes for different EP densities is shown. The base case represents the strongest scenario in the analysis, and the amplitude of the mode decreases after reaching its first peak. However, when the EP density is lowered, the amplitude evolution shows that it increases continuously after reaching its first peak. Once the amplitudes reach their maximum, they are damped and gradually decrease to a lower level. In figure 12, we measure the saturation scaling with the linear growth rate, where the saturation value is defined as the first peak, as in [49]. Since the saturation is caused by the flattening of the resonant particle density profile, in simulations without frequency chirping, the saturation can be distinguished as two mechanisms: quadratic scaling when saturation is caused by resonance detuning, and linear scaling when caused by radial decoupling.

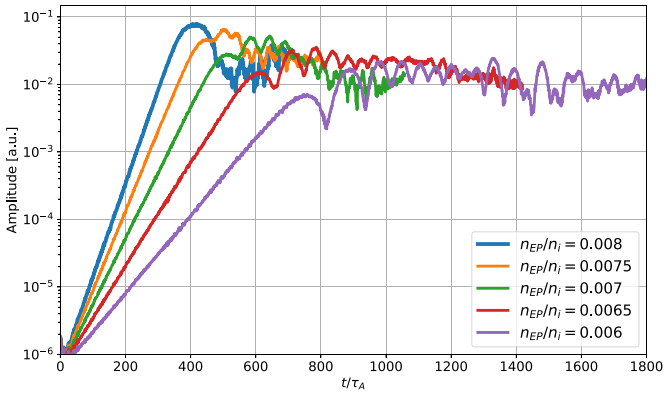

Figure 11. Time evolution of the mode amplitude at the peak for different EP densities.

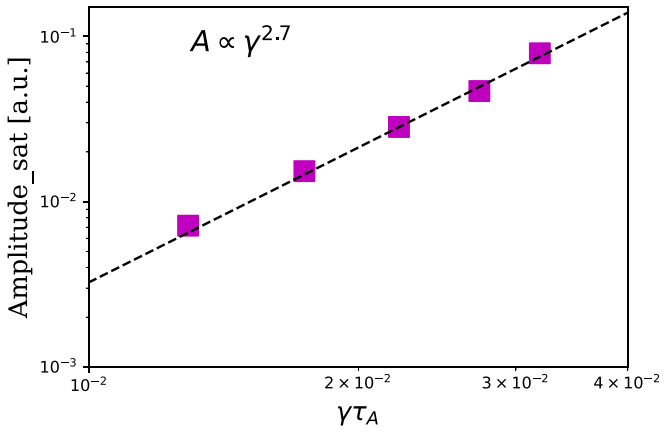

Figure 12. Scaling of saturation amplitude of scalar potential versus linear growth rate for EP density scan. Note that both coordinates are reported in logarithmic scale.

However, in the current simulations, the saturation amplitude in figure 12 is further enhanced and the scaling is stronger than that observed without frequency chirping. Such enhancing of saturation amplitude is expected due to the extension of wave-particle 'finite interaction time' by phase locking to the resonant particles and maximizing the power exchange with those particles [5].

In figure 13, the frequency spectrum for different EP density values is shown. As the EP density increases from left to right in the figure, the frequency chirping rate also increases as indicated by the increasing absolute value of the slope of the dashed fitting lines. This increase in chirping rate is proportional to the amplitude of the mode's saturation. Note the fundamental similarity between the behavior in figure 13 and the chirping of chorus events in the Earth's magnetosphere illustrated, e.g. in figure 11 of [75].

3.6. Background temperature gradient scan

In this section, we will consider five different temperature gradients corresponding to $\kappa_T = 0., 0.2, 0.4, 0.5, 0.6$, as shown in figure 14. This scan study is intended to establish reference single toroidal mode number simulations for future research on the dynamics of Alfvén modes in the presence of ITG turbulence. As shown in figure 14, the effective bulk plasma temperature decreases in the vicinity of the mode location by increasing κ_T.

In figure 15, the linear frequencies and growth rates of the mode obtained in simulations with different values of κ_T are presented. As the value of κ_T increases, the linear frequencies decrease while the growth rates increase. Figure 16 shows the linear mode radial mode structures of the normalized electrostatic potential in the upper panel and the frequency spectrum in the lower panel. The mode is linearly driven unstable around $s \simeq 0.7$, with a dominant $m = 8$ poloidal Fourier component for the electrostatic potential ϕ, and subdominant $m = 7$ and 9 components. The mode is located close to the lower accumulation point of a TAE gap on the shear Alfvén continuous spectrum. As κ_T increases, the mode moves deeper into the continuum where the local effective bulk plasma temperature decreases. Additionally, the $m = 8$ mode becomes relatively more dominant as the frequency decreases. By modifying the background plasma temperature gradient, the linear properties can be altered. Specifically, the local bulk plasma temperature varies across different cases, leading to differences in the shear Alfvén continuum. Consequently, the linear mode properties are expected to be modified, as predicted by the GFLDR in [3]. Figures 17 and 18 show that the saturation level increases for stronger modes and, consistently, the frequency chirping rates increase as the amplitude increases, as shown in figure 19. The saturation amplitude scaling with the linear growth rate, in particular, is analyzed in figure 18, where a cubic scaling is observed, consistent with the results obtained in the EP density scan. Note that, we only focused on the initial stage of nonlinear amplitude evolution because we observed frequency chirping during that time. However, the longer-term amplitude evolution may be affected by adding more physics, such as multi-mode interactions, collision and sources. Consequently, the chirping behaviours may change, which we will investigate in future work.

3.7. Frequency chirping rate vs. mode amplitude

Combining the simulation results so far, our analysis demonstrates that the frequency chirping rate of the mode is directly

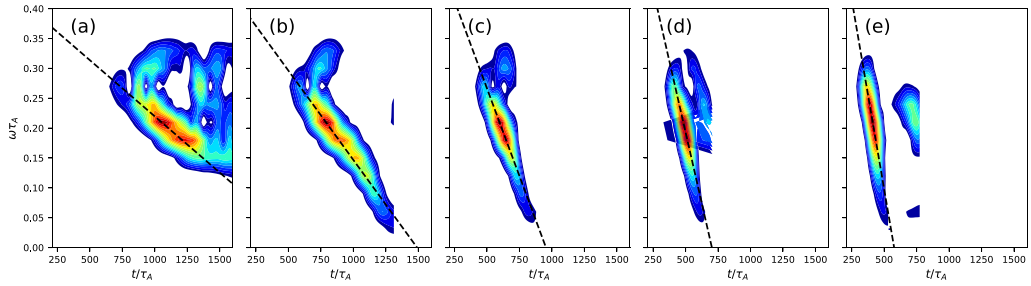

Figure 13. Frequency spectrum vs. time for different EP densities n_{EP0}/n_e with the values of (a) 0.006, (b) 0.0065, (c) 0.007, (d) 0.0075 and (e) 0.008, respectively.

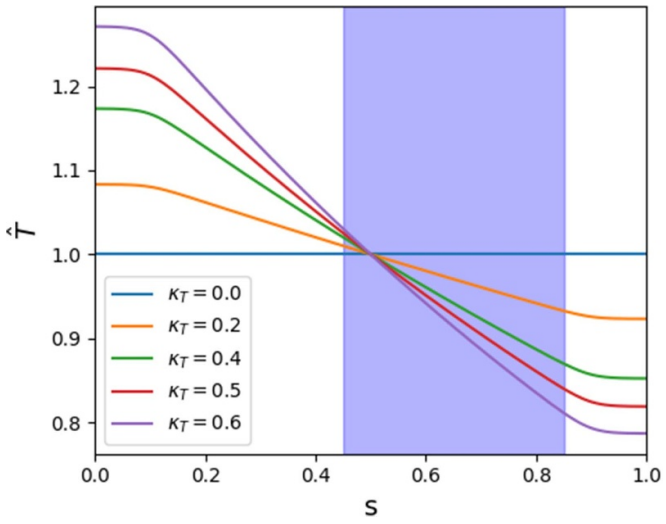

Figure 14. Normalized bulk plasma temperature profile for different κ_T.

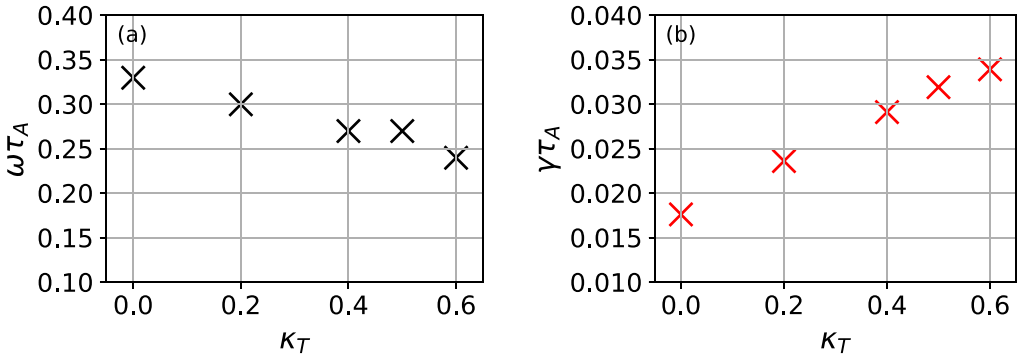

Figure 15. Mode real frequency in (a), and growth rate in (b) dependence of the temperature gradient defined by κ_T. EP density is retained with $n_{EP0}/n_e = 0.008$.

proportional to its saturation amplitude, as shown in figure 20. This holds true for all simulations conducted, despite variations in parameters such as EP density and temperature gradient. This evidence of linear scaling of the chirping rate with the mode amplitude is verification of the theoretical framework, originally proposed in [76] as a conjecture, and later developed into a unified self-consistent nonlinear theory [3–5, 26, 44, 77, 78], as indicated in equation (2). Considering that the same physics has been demonstrated by simulation results of chorus emission in the Earth's magnetosphere [1], consistent with the aforementioned general theoretical framework [2, 75], our present numerical analysis provides further support to the understanding of the features underlying frequency chirping phenomena in magnetized plasma due to non-perturbative wave-particle interactions. The small residual deviations of frequency chirping rate from linear dependence on the mode amplitude can be attributed to small variations in the mode's real frequency and radial structure, consistent with mode's linear properties in the considered nonuniform plasma equilibria.

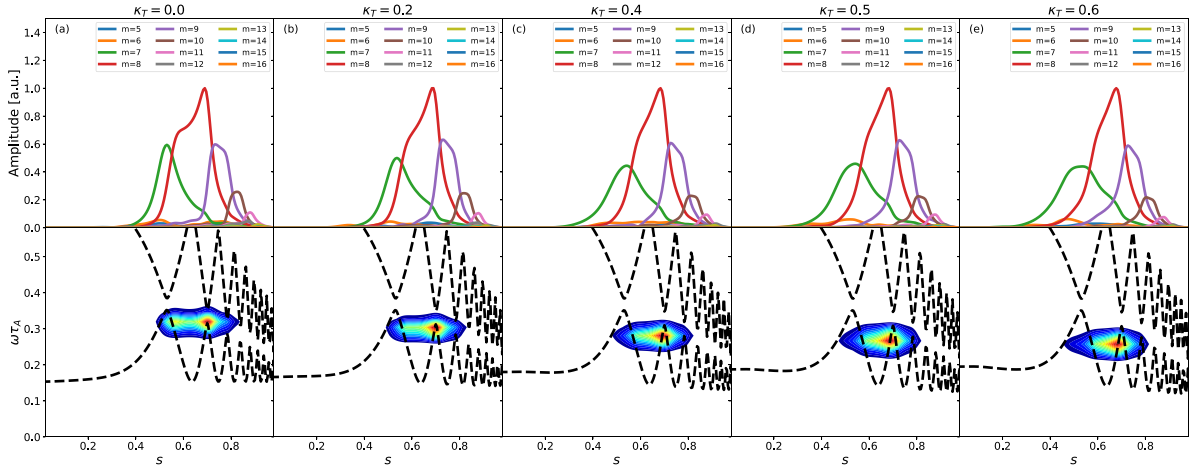

Figure 16. Linear radial structures of the poloidal harmonics of the mode on the top and frequency spectrum on the bottom for different values of κ_T.

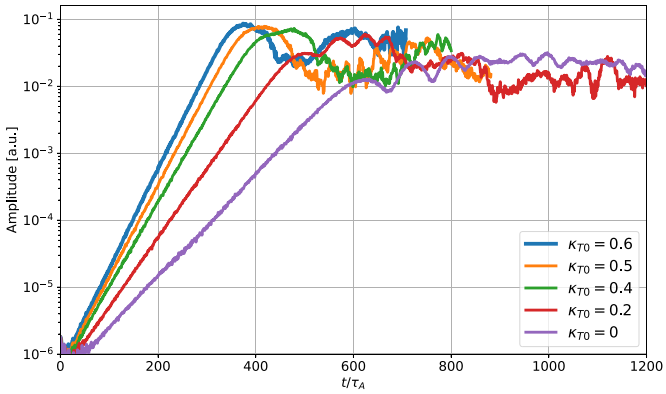

Figure 17. Time evolution of the mode amplitude at the peak for different values of κ_T.

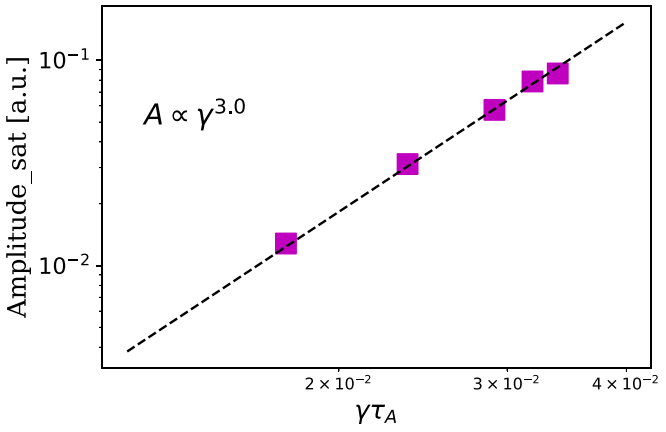

Figure 18. Scaling of saturation amplitude of scalar potential versus linear growth rate for different values of κ_T.

Note that our current simulations are focused on single-mode dynamics. As we consider more physics, such as multi-mode interactions, cross-scale couplings, sources and collision, the mode amplitude may be modified, and the particle dynamics will need to be further investigated in the future work.

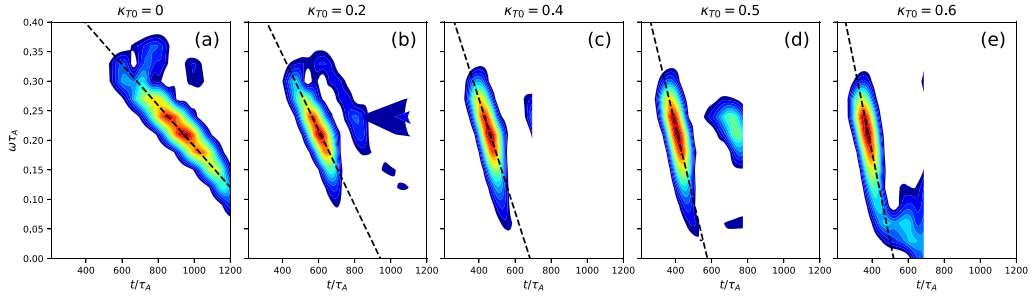

Figure 19. Frequency spectrum vs. time for different values of κ_T.

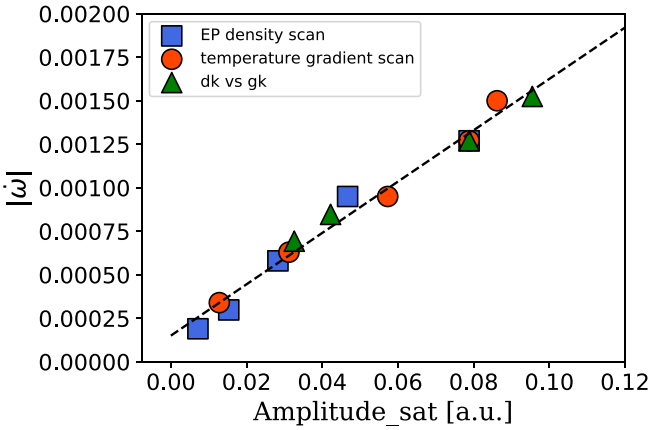

Figure 20. Frequency chirping rates vs. saturation amplitudes are shown, which are combining all the results from various parameter scans.

4. Conclusion

In this study, we analyze the frequency chirping of Alfvén modes in tokamak fusion plasmas that are driven by EPs using the global gyrokinetic PIC code ORB5. The existing unified and general theoretical framework provides predictions about the chirping rate, taking into account the non-perturbative impact of EPs on the mode structure and nonlinear frequency chirping. In section 2, We summarize the numerical evidence presented in [50]. Specifically, we discuss the concept of 'phase locking' together with non-perturbative EP response illuminates non-adiabatic frequency chirping at the condition for maximizing power exchange between the waves and EPs. The non-adiabatic frequency chirping can be characterized numerically by using the Finite Time Lyapunov Exponent analysis in the Hamiltonian mapping technique. We emphasize that particles are continously trapping and detrapping with respect to the resonance structure, which highlights the fundamental feature of the non-adiabatic chirping process; that is, the nonlinear chirping time scale is of the same order as the wave-particle trapping time. As a result, the frequency chirping rate dependence on saturation amplitude in the spontaneous evolution due to non-perturbative, self-consistent wave-particle nonlinear dynamics is different from an adiabatic chirping process controlled externally or by a slower perturbative process.

In this research, we use ORB5 simulations to examine the frequency chirping of an EPM under a fixed equilibrium and a single toroidal mode number. We vary models (drift- and gyro-kinetic) for the treatment of particle responses, and parameters such as, the density of EPs and the bulk plasma temperature gradients. Our findings show that an EPM can become unstable driven by an anisotropic EP distribution and then chirps along the shear Alfvén continuum with a self-consistently modified mode structure. By varying different parameters, we are able to change the mode saturation level. As a result, we observe that the frequency chirping rate also changes with the mode saturation level. We find that the frequency chirping rate is linearly dependent on the mode saturation amplitude, which is in agreement with the theoretical predictions of non-adiabatic chirping. We also argue that our result provide a strong support to the linear scaling of chirping rate with the flutuation amplitude as universal feature underlying frequency chirping phenomena in magnetized plasma due to non-perturbative wave-particle interactions. In fact, the universality of this linear dependence is recognized to be common in laboratory and space environments, with strong support from theory, simulation and experimental evidence.

Frequency chirping is a major concern in tokamaks due to its connection to fast ion losses, yet there is limited understanding on how to systematically avoid it. Our study in this paper provides evidence of non-adiabatic chirping features for a single toroidal mode, disregarding mode-mode couplings. By identifying the dynamics of single toroidal mode frequency chirping, our study can serve as a reference case for more complex conditions. Using the comprehensive physical model implemented in the gyrokinetic code ORB5, we can further investigate chirping dynamics starting from the current reference cases. Future investigations will focus on how resonance overlap, zonal flows, or cross-scale couplings with plasma turbulence [79] may modify the chirping dynamics.

Data availability statement

Permission is needed to access the code that is used to produce the data. The data that support the findings of this study are available upon reasonable request from the authors.

Acknowledgments

This work has been carried out within the framework of the EUROfusion Consortium, partially funded by the European Union via the Euratom Research and Training Programme (Grant Agreement No. 101052200 - EUROfusion). The Swiss contribution to this work has been funded by the Swiss State Secretariat for Education, Research and Innovation (SERI). Views and opinions expressed are however those of the author(s) only and do not necessarily reflect those of the European Union, the European Commission or SERI. Neither the European Union nor the European Commission nor SERI can be held responsible for them. Simulations presented in this work were performed on the MARCONI FUSION HPC system at CINECA.

ORCID iDs

X Wang https://orcid.org/0000-0002-3756-1771
M Falessi https://orcid.org/0000-0002-2105-226X
T Hayward-Schneider https://orcid.org/0000-0003-0588-5090
A Mishchenko https://orcid.org/0000-0003-1436-4502
L Villard https://orcid.org/0000-0003-3807-9482
F Zonca https://orcid.org/0000-0002-9270-4704

References

[1] Tao X, Zonca F and Chen L 2021 A "trap-release-amplify" model of chorus waves *J. Geophys. Res. Space Phys.* **126** e2021JA029585
[2] Zonca F, Tao X and Chen L 2022 A theoretical framework of chorus wave excitation *J. Geophys. Res. Space Phys.* **127** e2021JA029760
[3] Chen L and Zonca F 2016 Physics of Alfvén waves and energetic particles in burning plasmas *Rev. Mod. Phys.* **88** 015008
[4] Chen L and Zonca F 2013 On nonlinear physics of shear Alfvén waves *Phys. Plasmas* **20** 055402
[5] Zonca F, Chen L, Briguglio S, Fogaccia G, Vlad G and Wang X 2015 Nonlinear dynamics of phase space zonal structures and energetic particle physics in fusion plasmas *New J. Phys.* **17** 013052
[6] Berk H L and Breizman B N 1990 Saturation of a single mode driven by an energetic injected beam. II. Electrostatic "universal" destabilization mechanism *Phys. Fluids* B **2** 2235–45
[7] Berk H L and Breizman B N 1990 Saturation of a single mode driven by an energetic injected beam. III. Alfvén wave problem *Phys. Fluids* B **2** 2246–52
[8] O'Neil T 1965 Collisionless damping of nonlinear plasma oscillations *Phys. Fluids* **8** 2255–62
[9] O'Neil T M, Winfrey J H and Malmberg J H 1971 Nonlinear interaction of a small cold beam and a plasma *Phys. Fluids* **14** 1204–12
[10] Berk H L and Breizman B N 1990 Saturation of a single mode driven by an energetic injected beam. I. plasma wave problem *Phys. Fluids* B **2** 2226–34
[11] Berk H L, Breizman B N and Ye H 1992 Scenarios for the nonlinear evolution of alpha-particle-induced Alfvén wave instability *Phys. Rev. Lett.* **68** 3563–6
[12] Berk H L, Breizman B N, Fitzpatrick J, Pekker M S, Wong H V and Wong K L 1996 Nonlinear response of driven systems in weak turbulence theory *Phys. Plasmas* **3** 1827–38
[13] Breizman B N, Berk H L, Pekker M S, Porcelli F, Stupakov G V and Wong K L 1997 Critical nonlinear phenomena for kinetic instabilities near threshold *Phys. Plasmas* **4** 1559–68
[14] Berk H, Breizman B and Petviashvili N 1997 Spontaneous hole-clump pair creation in weakly unstable plasmas *Phys. Lett.* A **234** 213–8
[15] Berk H L, Breizman B N, Candy J, Pekker M and Petviashvili N V 1999 Spontaneous hole-clump pair creation *Phys. Plasmas* **6** 3102–13
[16] Fasoli A, Breizman B N, Borba D, Heeter R F, Pekker M S and Sharapov S E 1998 Nonlinear splitting of fast particle driven waves in a plasma: observation and theory *Phys. Rev. Lett.* **81** 5564–7
[17] Pinches S D, Berk H L, Gryaznevich M P, Sharapov S E and Contributors J-E 2004 Spectroscopic determination of the internal amplitude of frequency sweeping TAE *Plasma Phys. Control. Fusion* **46** S47
[18] Vann R G L, Dendy R O and Gryaznevich M P 2005 Theoretical interpretation of frequency sweeping observations in the mega-amp spherical tokamak *Phys. Plasmas* **12** 032501
[19] Gryaznevich M and Sharapov S 2006 Perturbative and non-perturbative modes in start and mast *Nucl. Fusion* **46** S942
[20] Bernstein I B, Greene J M and Kruskal M D 1957 Exact nonlinear plasma oscillations *Phys. Rev.* **108** 546–50
[21] Breizman B N 2010 Nonlinear travelling waves in energetic particle phase space *Nucl. Fusion* **50** 084014
[22] Breizman B 2011 Nonlinear consequences of energetic particle instabilities *Fusion Sci. Technol.* **59** 549–60
[23] Breizman B N and Sharapov S E 2011 Major minority: energetic particles in fusion plasmas *Plasma Phys. Control. Fusion* **53** 054001
[24] Lilley M and Breizman B 2012 Convective transport of fast particles in dissipative plasmas near an instability threshold *Nucl. Fusion* **52** 094002
[25] Lilley M K and Nyqvist R M 2014 Formation of phase space holes and clumps *Phys. Rev. Lett.* **112** 155002
[26] Zonca F, Briguglio S, Chen L, Fogaccia G and Vlad G 2005 Transition from weak to strong energetic ion transport in burning plasmas *Nucl. Fusion* **45** 477
[27] Zonca F *et al* 2007 Electron fishbones: theory and experimental evidence *Nucl. Fusion* **47** 1588
[28] Lanti E *et al* 2020 Orb5: a global electromagnetic gyrokinetic code using the pic approach in toroidal geometry *Comput. Phys. Commun.* **251** 107072
[29] Heidbrink W W 2008 Basic physics of Alfvén instabilities driven by energetic particles in toroidally confined plasmas *Phys. Plasmas* **15** 055501
[30] White R B, Goldston R J, McGuire K, Boozer A H, Monticello D A and Park W 1983 Theory of mode-induced beam particle loss in tokamaks *Phys. Fluids* **26** 2958–65
[31] Chen L, White R B and Rosenbluth M N 1984 Excitation of internal kink modes by trapped energetic beam ions *Phys. Rev. Lett.* **52** 1122–5
[32] Chen L 1999 Theory of plasma transport induced by low-frequency hydromagnetic waves *J. Geophys. Res. Space Phys.* **104** 2421–7
[33] White R B, Gorelenkov N, Heidbrink W W and Van Zeeland M A 2010 Beam distribution modification by Alfvén modes *Phys. Plasmas* **17** 056107
[34] White R B, Gorelenkov N, Heidbrink W W and Zeeland M A V 2010 Particle distribution modification by

low amplitude modes *Plasma Phys. Control. Fusion* **52** 045012
[35] Falessi M V and Zonca F 2019 Transport theory of phase space zonal structures *Phys. Plasmas* **26** 022305
[36] Zonca F, Chen L, Falessi M V and Qiu Z 2021 Nonlinear radial envelope evolution equations and energetic particle transport in tokamak plasmas *J. Phys.: Conf. Ser.* **1785** 012005
[37] Berk H L, Nielsen C E and Roberts K V 1970 Phase space hydrodynamics of equivalent nonlinear systems: experimental and computational observations *Phys. Fluids* **13** 980–95
[38] Dupree T H 1970 Theory of resistivity in collisionless plasma *Phys. Rev. Lett.* **25** 789–92
[39] Dupree T H 1972 Theory of phase space density granulation in plasma *Phys. Fluids* **15** 334–44
[40] Dupree T H 1982 Theory of phase-space density holes *Phys. Fluids* **25** 277–89
[41] Tetreault D J 1983 Growth rate of the clump instability *Phys. Fluids* **26** 3247–61
[42] Mynick H and Pomohrey N 1994 Frequency sweeping: a new technique for energy-selective transport *Nucl. Fusion* **34** 1277
[43] Escande D F, Bénisti D, Elskens Y, Zarzoso D and Doveil F 2018 Basic microscopic plasma physics from n-body mechanics *Rev. Mod. Plasma Phys.* **2** 9
[44] Zonca F, Chen L, Briguglio S, Fogaccia G, Milovanov A V, Qiu Z, Vlad G and Wang X 2014 Energetic particles and multi-scale dynamics in fusion plasmas *Plasma Phys. Control. Fusion* **57** 014024
[45] Carlevaro N, Falessi M, Montani G and Zonca F 2015 Nonlinear physics and energetic particle transport features of the beam-plasma instability *J. Plasma Phys.* **81** 495810515
[46] Peacock T and Haller G 2013 Lagrangian coherent structures:: the hidden skeleton of fluid flows *Phys. Today* **66** 41
[47] Falessi M, Pegoraro F and Schep T 2015 Lagrangian coherent structures and plasma transport processes *J. Plasma Phys.* **81** 495810505
[48] Di Giannatale G, Falessi M V, Grasso D, Pegoraro F and Schep T J 2018 Coherent transport structures in magnetized plasmas. I. theory *Phys. Plasmas* **25** 052306
[49] Briguglio S, Wang X, Zonca F, Vlad G, Fogaccia G, Di Troia C and Fusco V 2014 Analysis of the nonlinear behavior of shear Alfvén modes in tokamaks based on hamiltonian mapping techniques *Phys. Plasmas* **21** 112301
[50] Wang X, Briguglio S, Di Troia C, Falessi M, Fogaccia G, Fusco V, Vlad G and Zonca F 2022 Analysis of the nonlinear dynamics of a chirping-frequency Alfvén mode in a tokamak equilibrium *Phys. Plasmas* **29** 032512
[51] Zonca F and Chen L 1996 Theory of toroidal Alfvén modes excited by energetic particles in tokamaks *Phys. Plasmas* **3** 323–43
[52] Chen L and Zonca F 1995 Theory of shear Alfvén waves in toroidal plasmas *Phys. Scr.* **1995** 81
[53] Briguglio S, Vlad G, Zonca F and Kar C 1995 Hybrid magnetohydrodynamic-gyrokinetic simulation of toroidal Alfvén modes *Phys. Plasmas* **2** 3711–23
[54] Briguglio S, Zonca F and Vlad G 1998 Hybrid magnetohydrodynamic-particle simulation of linear and nonlinear evolution of Alfvén modes in tokamaks *Phys. Plasmas* **5** 3287–301
[55] Chen L 1994 Theory of magnetohydrodynamic instabilities excited by energetic particles in tokamaks *Phys. Plasmas* **1** 1519–22
[56] Zonca F and Chen L 2000 Destabilization of energetic particle modes by localized particle sources *Phys. Plasmas* **7** 4600–8
[57] Wang Z, Lin Z, Holod I, Heidbrink W W, Tobias B, Van Zeeland M and Austin M E 2013 Radial localization of toroidicity-induced Alfvén eigenmodes *Phys. Rev. Lett.* **111** 145003
[58] Fajans J and Friédland L 2001 Autoresonant (nonstationary) excitation of pendulums, plutinos, plasmas and other nonlinear oscillators *Am. J. Phys.* **69** 1096–102
[59] Meerson B and Friedland L 1990 Strong autoresonance excitation of rydberg atoms: the rydberg accelerator *Phys. Rev.* A **41** 5233–6
[60] Wang G 2013 *PhD Thesis* University of Texas, Austin, tx
[61] Wang G and Berk H 2012 Simulation and theory of spontaneous tae frequency sweeping *Nucl. Fusion* **52** 094003
[62] Wang X, Briguglio S, Chen L, Di Troia C, Fogaccia G, Vlad G and Zonca F 2012 Nonlinear dynamics of beta-induced Alfvén eigenmode driven by energetic particles *Phys. Rev.* E **86** 045401
[63] Vlad G, Briguglio S, Fogaccia G, Zonca F, Fusco V and Wang X 2013 Electron fishbone simulations in tokamak equilibria using xhmgc *Nucl. Fusion* **53** 083008
[64] Jolliet S, Bottino A, Angelino P, Hatzky R, Tran T, Mcmillan B, Sauter O, Appert K, Idomura Y and Villard L 2007 A global collisionless pic code in magnetic coordinates *Comput. Phys. Commun.* **177** 409–25
[65] Bottino A, Vernay T, Scott B, Brunner S, Hatzky R, Jolliet S, McMillan B F, Tran T M and Villard L 2011 Global simulations of tokamak microturbulence: finite-β effects and collisions *Plasma Phys. Control. Fusion* **53** 124027
[66] Tronko N, Bottino A and Sonnendrücker E 2016 Second order gyrokinetic theory for particle-in-cell codes *Phys. Plasmas* **23** 082505
[67] Mishchenko A *et al* 2019 Pullback scheme implementation in orb5 *Comput. Phys. Commun.* **238** 194–202
[68] Rettino B, Hayward-Schneider T, Biancalani A, Bottino A, Lauber P, Chavdarovski I, Weiland M, Vannini F and Jenko F 2022 Gyrokinetic modeling of anisotropic energetic particle driven instabilities in tokamak plasmas *Nucl. Fusion* **62** 076027
[69] Stix T H 1972 Heating of toroidal plasmas by neutral injection *Plasma Phys.* **14** 367
[70] Cheng C Z and Chance M S 1986 Low-n shear Alfvén spectra in axisymmetric toroidal plasmas *Phys. Fluids* **29** 3695–701
[71] Chu M S, Greene J M, Lao L L, Turnbull A D and Chance M S 1992 A numerical study of the high-n shear Alfvén spectrum gap and the high-n gap mode *Phys. Fluids* B **4** 3713–21
[72] Zonca F, Chen L and Santoro R A 1996 Kinetic theory of low-frequency Alfvén modes in tokamaks *Plasma Phys. Control. Fusion* **38** 2011
[73] Biancalani A, Bottino A, Briguglio S, Könies A, Lauber P, Mishchenko A, Poli E, Scott B D and Zonca F 2016 Linear gyrokinetic particle-in-cell simulations of Alfvén instabilities in tokamaks *Phys. Plasmas* **23** 012108
[74] Mishchenko A, Könies A and Hatzky R 2009 Global particle-in-cell simulations of fast-particle effects on shear Alfvén waves *Phys. Plasmas* **16** 082105
[75] Zonca F, Tao X and Chen L 2021 Nonlinear dynamics and phase space transport by chorus emission *Rev. Mod. Plasma Phys.* **5** 8

[76] Zonca F and Chen L 2000 Destabilization of energetic par- article modes by icrf induced fast minority ion tails on tftr *Proc. 6th IAEA TCM on Ener- Getic Particles in Magnetic Confinement Systems, JAERI-Conf. 2000-004* p 52

[77] Zonca F, Briguglio S, Chen L, Fogaccia G, Hahm T S, Milovanov A V and Vlad G 2006 Physics of burning plasmas in toroidal magnetic confinement devices *Plasma Phys. Control. Fusion* **48** B15

[78] Chen L and Zonca F 2007 Theory of Alfvén waves and energetic particle physics in burning plasmas *Nucl. Fusion* **47** S727

[79] Duarte V, Berk H, Gorelenkov N, Heidbrink W, Kramer G, Nazikian R, Pace D, Podestá M, Tobias B and Zeeland M V 2017 Prediction of nonlinear evolution character of energetic-particle-driven instabilities *Nucl. Fusion* **57** 054001